DOI: 10.13009/EUCASS2019-201

Effect of pressure gradient on stability of small disturbances in supersonic boundary-layer flows

P.V. Chuvakhov[*ab], *A.O. Obraz*[**ab], *E.A. Alexandrova*[***a], *A.V. Fedorov*[****ba], *I.V. Egorov*[*****ab]

[a]*Central Aerohydrodynamic Institute (TsAGI), 1 Zhukovskogo Str., Zhukovsky, 140180, Russia*
[b]*Moscow Institute of Physics and Technology (MIPT), 9 Institutskiy Per., Dolgopridny, 141701, Russia*
[*] *pavel_chuvakhov@mail.ru*
[**] *obraz.ao@mipt.ru*
[***] *miptjane@gmail.com*
[****] *fedorov@falt.ru*
[*****] *ivan.egorov@tsagi.ru*

Abstract

The effect of pressure gradient on stability of small disturbances is investigated using the linear stability theory. A flow past plain expansion corners with different angles is considered at Mach 6. The amplification of the disturbances in the boundary layer is computed using e-N method. The strong stabilizing effect of the expansion is observed numerically.

1. Introduction

The flow over supersonic and hypersonic aircraft elements (segmental-conical fairings, rudders, shields, elevons, flat joints of external geometry, nozzles, etc.) is associated with the formation of accelerating and decelerating flow regions, where the boundary layer may separete, interacting with shock waves, and form zones of increased heat transfer with subsequent attachment to the surface. The boundary layer turbulization greatly enhances this effect. Accelerating flow regions with a favorable (negative) pressure gradient occur in practice as often as deceleration zones. Despite this, the majority of computational, theoretical and experimental studies are devoted to decelerating flows, such as supersonic flow in a compression angle. The fundamental problem of the influence of a favorable pressure gradient on the stability of the laminar boundary layer and the relaminarization of the turbulent boundary layer is much less studied. This gap is especially noticeable for hypersonic flow regimes. There are several experimental studies confirming stabilization effect of the favorable pressure gradient, but there are practically no theoretical and computational studies of the mechanisms underlying it.

Relaminarization of a high-speed turbulent boundary layer is associated with a significant decrease in heat loads on the aircraft elements. Therefore, an understanding of the basic process mechanisms of suppression of disturbances and turbulence in the accelerating flow regions will help predict the turbulence occurrence and optimize the thermal protection of high-speed aircraft of the new generation.

The problem of the turbulent flow returning to the laminar state (relaminarization) has been studied since the middle of the last century. The investigation of subsonic turbulent flows in the presence of a large negative pressure gradient indicated the possibility of complete boundary layer relaminarization [1-4], which is associated with the curved nature of the streamline, as well as favorable longitudinal and normal pressure gradients, leading to a rapid reduction in the scale of turbulent pulsations in the accelerating flow region [5]. The magnitude of the longitudinal static pressure gradient and the free-stream Reynolds number were noted as the main flow parameters affecting the relaminarization process. On the basis of these quantities and parameters characterizing the boundary layer state, various criteria for the relaminarization onset are proposed. Relaminarization in a supersonic flow regime leads to a significant weakening of heat transfer from the hot gas to the streamlined surface. Today there is a large amount of experimental evidence that compressibility effects prevail over other effects in the external part of the boundary layer (for example, [6, 7]). The compressibility effect, in particular, includes weak damping and an increase of the size of large-scale vortex structures in expansion flow at Mach number 3 [6]. In addition, a significant suppression of Reynolds shear stresses was noted in [6], as a result of which large-scale structures are weakened downstream. In a number of studies (including [6]), there is a significant suppression of small-scale structures immediately behind a fan of rarefaction waves. These conclusions are confirmed in experiments with Mach number 4.9 [8, 9]. In these studies, it was also found that the region of the boundary layer intermittency in the accelerating flow is reduced, shifting to its boundary. This makes it difficult to mix gas from an external flow into the boundary layer.

DOI: 10.13009/EUCASS2019-201

Experimental studies of relaminarization are also conducted in Russia. It is shown in Novosibirsk (ITAM) at Mach numbers from 2 to 4 [10] that partial relaminarization of the boundary layer is possible (near-wall part up to 40% of full thickness). It was also noted that the Reynolds number increase mainly leads to an increase of the length of the relaminarized flow section, and a greater flow acceleration (greater negative pressure gradient) in the interaction region leads to greater decrease of turbulent pulsations. According to the results, it was concluded that relaminarization criteria obtained at subsonic velocities can be applied at high supersonic velocities. Experiments were carried out in Zhukovsky (TsAGI) in wind tunnels in the range of Mach numbers from 5 to 8. They indirectly confirm the stabilizing effect of the favorable pressure gradient on the body of revolution " ogive-cone-cone-cylinder", as well as on turbulent wedge relaminarization behind a single surface roughness [11].

Experimental studies (for example, [9]) provide a good test base for the development of RANS and LES computational models for this type of flows. However, there are very few publications on direct numerical simulation of the relaminarization phenomenon in supersonic flow regimes due to computational complexity. The authors know only the studies [12] at Mach number M = 2.9 and [13] at Mach number M = 2.7. A turbulent flow around the rarefaction angle was considered in both papers. A two-layer structure of the accelerating flow near the angle was found, confirming the experimental observations. The flow in the upper layer is characterized by a strong suppression of turbulent pulsations, which are slowly restored downstream. In the lower layer, the pulsations are suppressed only in a small vicinity near the turning point and are quickly restored downstream. The authors are not aware of similar studies at high supersonic and hypersonic velocities. It should be noted that the applicability of the relaminarization criteria at a Mach number above three is questioned in computations by the RANS method [14]. An insignificant number of papers at large Mach numbers does not allow us to obtain the necessary corrections for compressibility. In this regard, the importance of research in this area is emphasized. The evolution of a developed turbulent boundary layer in the region of a favorable pressure gradient is a complex task, which depends on many factors. In this study, an attempt is made to isolate these factors within the framework of the linear stability theory and in this way to study the mechanisms underlying the relaminarization phenomenon in hypersonic flow regimes.

It is known that the process of a hypersonic flow transition into a turbulent state on a smooth surface in quiet conditions of hypersonic flight occurs through the formation, growth and merge of individual turbulent spots. The turbulent spot formation occurs under different scenarios depending on the undisturbed flow parameters, the background of disturbances and the temperature of the streamlined surface. According to the linear stability theory, the inclined waves of the first mode dominate over the hot (heat insulated) surface; the plane waves of the second mode dominate above the cooled surface. Although the turbulent spot is a substantially non-linear object, its development is influenced by linear stability mechanisms. Previous computations [15] reveal a relationship between the characteristics of turbulent spots and linear wave packets. There are a number of experimental and numerical studies (a detailed review is given in [15]), which confirm these results.

It should be noted that the shapes and dynamic properties of turbulent spots in hypersonic flow regimes are poorly studied. To date, there are a small number of experiment-computed studies on the evolution of turbulent spots and wave packets in a hypersonic boundary layer on simple configuration bodies: a flat plate, a cone, a compression angle. And direct numerical simulation of turbulent spots on a plate at Mach 6 was performed in [16]. It is shown that the spot shape substantially depends on the temperature of the streamlined surface: the spots are strongly extended along the flow on the cooled wall, and they have a classic triangular shape on the heat-insulated wall. As far as the authors of this studies are aware, the evolution of spots at supersonic and hypersonic flow velocities in areas of favorable pressure gradient, such as a rarefaction angle, has not been studied enough. Estimated computations performed by the paper authors earlier for configurations such as axisymmetric rarefaction angle show that the instability of the hypersonic boundary layer is suppressed when the flow turns from the conical part to the cylindrical part of the surface.

This study is devoted to the investigation of the stabilization (relaminarization) mechanisms of turbulent flow under the action of a favorable pressure gradient within the framework of the linear stability theory. The fundamental problem of the development of small disturbances (wave packets) in the boundary layer at a rarefaction angle at the Mach number 6 is considered. The study of this issue will allow to set tasks of the direct numerical simulation of the development of wave packets and turbulent spots when flowing around the rarefaction angle, which will later allow to create the basis for a generalization of the intermittency models describing laminar-turbulent transition at hypersonic flow velocities on gradient hypersonic flows.The authors of this study have already taken the first step in this direction [17].

2. Formulation of linear stability problem

Propagation of the disturbances through the expansion corner was modelled within the Linear Stability Theory (LST) framework, briefly discussed here. The small disturbances $\mathbf{Q}'(\mathbf{x},t)$ are introduced into the mean flow $\overline{\mathbf{Q}}(\mathbf{x})$:

DOI: 10.13009/EUCASS2019-201

$$\mathbf{Q}(\mathbf{x},t) = \overline{\mathbf{Q}}(\mathbf{x}) + \mathbf{Q}'(\mathbf{x},t) \tag{1}$$

Here $\mathbf{Q}$ is the vector of gas-dynamics values at a given point $\mathbf{Q} = \{u, v, w, p, T\}$, u, v, w - components of the velocity vector in the global Cartesian reference frame, p - pressure, T - temperature. The substitution of (1) into Navier-Stokes equations provides a system of nonlinear partial differential equation for the disturbance field if the mean flow is known. The system can be greatly simplified in the case of boundary layer problems when the disturbance can be expanded as follows (for a two-dimensional case $\mathbf{x} = \{x, y\}^T$):

$$\mathbf{Q}'(x,y,t) = \frac{1}{2\pi}\int_0^\infty \exp(-i\omega t)\int_{-\infty}^{\infty} \exp(i\alpha x)\hat{\mathbf{q}}(y;\alpha,\omega)d\alpha d\omega \tag{2}$$

Here the elemental disturbances has the form of the travelling wave with the frequency ω and streamwise wavenumber α:

$$\mathbf{q}(x,y,t;\alpha,\omega) = \hat{\mathbf{q}}(y;\alpha,\omega)\exp(i\alpha x - i\omega t) \tag{3}$$

If the disturbances are considered small ($\|\mathbf{Q}'\| / \|\overline{\mathbf{Q}}\| << 1$), the substitution of (3) in the stability system of equations produces the system of ordinary differential equations:

$$(AD^2 + BD + C)\hat{\mathbf{q}} = 0 \tag{4}$$

Here $D = \dfrac{\partial}{\partial y}$, matrices A, B, C in two-dimensional case are square 4x4 matrices depending on the mean flow $\overline{\mathbf{Q}}(x,y)$ and the characteristics of the disturbance α, ω. The system (4) should be closed by a set of boundary conditions. In this work the propagation of unstable boundary layer enigenmodes is considered through the expansion corner. These modes of discrete spectrum (see Section 4) have the following set of boundary conditions:

$$\begin{aligned} &y = 0 : \hat{q}_1, \hat{q}_2, \hat{q}_3, \hat{q}_5 = 0, \\ &y \to \infty : \hat{q}_1, \hat{q}_2, \hat{q}_3, \hat{q}_5 \to 0. \end{aligned} \tag{5}$$

The first set of conditions states that velocity disturbances at the wall vanish, and also the thermal impermeability of the wall. The second set states that the disturbances' amplitude functions decay far outside the boundary layer.

The system (4) with the uniform boundary condition (5) formulates the eigenvalue task. That means that the non-trivial solutions for the set of amplitude functions $\hat{\mathbf{q}}(y)$ exists only when the dispersion relation between frequency ω and wave-number α is satisfied:

$$F(\omega,\alpha) = 0 \tag{6}$$

If for a given pair $(\tilde{\omega}, \tilde{\alpha})$ the condition (6) is satisfied, an eigenmode with a corresponding set of amplitude functions is found. There are several approaches to solve (6) numerically. The stability task can be solved in spatial or temporal approach. In the first case, α is considered complex and ω is considered real. In the second case, ω is considered complex and α is considered real. The first approach seems more correlated with the spatially growing disturbances, for this reason all the computations in this work performed with spatial formulation.

The first method of solving (6) developed in [18] is to reduce the system (6) to the system of first-order equations with the new vector of unknowns

$$\tilde{\mathbf{q}} = \{q_u, q_{du/dy}, q_v, q_p, q_T, q_{dT/dy}\}^T = \{q_1, ..., q_6\}^T. \tag{7}$$

The system (4) is then rewritten in the following form:

$$\frac{d\tilde{\mathbf{q}}}{dy} = \mathbf{B}\tilde{\mathbf{q}} \tag{8}$$

DOI: 10.13009/EUCASS2019-201

Here the matrix **B** also depends on mean-flow values and characteristics of the disturbance.The one-dimensional computational domain usually contains several thicknesses of boundary layer. In this work the integration of (8) is performed numerically with the Runge-Kutta scheme of 4th order of approximation with an orthogonalization of basic functions to avoid numerical singularities. This enables to calculate the value F from (6) for a given pair of (ω,α). The equation (6) is solved numerically using the Newton method when ω is fixed and eigenvalue α is sought. It is to mention here that this method requires a good initial approach for the eigenvalue which is a common requirement for the Newton method to converge.

Another method of solving (6) is to solve (4) directly with spectral methods. If the global vector of unknowns in (4) is written for the discretized system $q_g = (q_1^{(1)}, q_2^{(1)}, q_3^{(1)}, q_4^{(1)}, ..., q_1^{(N)}, q_2^{(N)}, q_3^{(N)}, q_4^{(N)})$, the system (4) can be rewritten in the form

$$\mathbf{M}\alpha^2 + \mathbf{A}_\alpha\alpha = \mathbf{B}_\alpha \tag{9}$$

The matrices $\mathbf{M}, \mathbf{A}_\alpha, \mathbf{B}_\alpha$ are square sparse matrices of large dimensions (4Nx4N) where N is the number of grid points in the discretization. The square term in (9) with all the terms divided by the Reynolds number can be often neglected which produces a generalized linear eigenvalue problem

$$\mathbf{A}_\alpha\alpha = \mathbf{B}_\alpha \tag{10}$$

The spectrum of (10) can be found numerically using various linear algebra routines. The original method of solving the system (4) as (9) was proposed in [19]. In this work the method was implemented with the help of QR-decomposition method from the LAPACK library. This procedure allows to produce the full spectrum of the boundary layer at a given point with both discrete and continuous modes for a fixed frequency. This is an important tool in the case when several discrete modes are present in the spectrum and the eigenvalues of α can also be used as initial approaches for the integration method.

The numerical solution of (8) or (10) provides the local growth rates of the disturbances at a given point $\sigma = -\alpha_i$. The integration of the growth rate provides the logarithm of the amplification of the disturbance from its origin:

$$N \equiv \ln\left(\frac{|Q|}{|Q_0|}\right) = \int_{x_0}^{x} \sigma(\xi) d\xi \tag{11}$$

This is the basic idea of the so-called e-N method [20], [21], which is well-developed for the last 50 years and is the most physically-based engineering tool for computation of the amplification of disturbances in the boundary layer. The integration in (11) in this work is performed for a set of plane disturbances (see Section 3) of fixed frequencies, the locations x_0 correspond to the neutral point of the disturbances.

3. Configuration of the mean flow

In this work the propagation of disturbances along the surface of expansion ramp is considered. Figure 1 shows the temperature flowfield for the case of expansion $\theta = 10^0$. The non-dimensional temperature value is presented: $T = T^* / T_\infty^*$. Here T^* is the dimensional value, T_∞^* is the dimensional free-stream value. The parameters that are fixed for all cases considered are as follows: the free-stream Mach number is 6, the wall temperature is 150K, the free-stream temperature is 73.2K. These parameters correspond to the relatively cold wall. At these conditions usually the second mode disturbances are dominant in the boundary layer. The Reynolds number computed over the characteristic length $L = 0.1m$ is $\mathrm{Re}_L = 10^6$. The geometry scales at Figure 1 are non-dimensional and obtained as follows: $x = x^* / L, y = y^* / L$. The flat-plate section before the expansion is 0.75m long and the expansion part is 0.75m long.

The mean laminar flowfields over the expansion corner were computed using the in-house code HSFlow [22]. The stationary flow fields were obtained by marching in time with the TVD (Total Variation Diminishing) scheme that has the second-order of accuracy in space and time. A fine two-dimensional strucutred meshes were used with an average number of grid nodes 800x600 in streamwise and wall-normal directions, correspondingly. Approximately 250 grid nodes were inside the boundary layer at the point where expansion starts (point *x=0, y=0* at Figure 1). The viscosity was calculated using the Sutherland's law with the constant $T_s = 110.4K$, Prandtl number was fixed $\mathrm{Pr} = 0.72$.

DOI: 10.13009/EUCASS2019-201

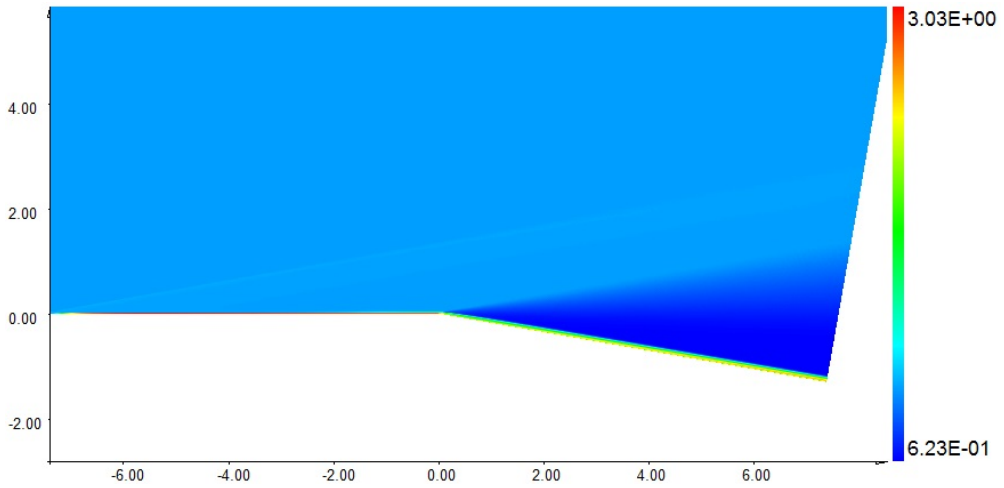

Figure 1: Temperature flowfield over the expansion ramp ($\theta = 10^0$).

The following angles of the expansion were considered: $\theta = 0^0; 5^0; 10^0; 15^0$. The first case corresponds to the flat-plate flow. For all cases considered e-N calculations were performed with the computed flowfields. Within the locally parallel LST-framework, the stability of the boundary layer depends on the local boundary-layer profiles extracted at a given point. Here we provide some analysis on the mean flow profiles along the inviscid steamline on the boundary layer edge. Figure 2 provides the profiles of temperature in the boundary layer at various x-stations. It is seen that before the expansion corner the profile has a typical flat-plate distribution. After the corner there is a region where the inviscid expansion flow resides at the upper edge of the boundary layer, modifying it drastically (section *x=0.3*). Far away from the corner the boundary layer and inviscid expansion flow split, and the temperature profile again resemble that of the flat plate, although the edge temperature changes significantly. Thus, the region of the flow near the corner has a rapid variation of boundary layer thickness and profiles, which is the reason for the complex disturbance spectrum in that region (section 5). The strong connection between the boundary layer flow and the inviscid expansion flow is observed in the region $0 < x < 1.0$.

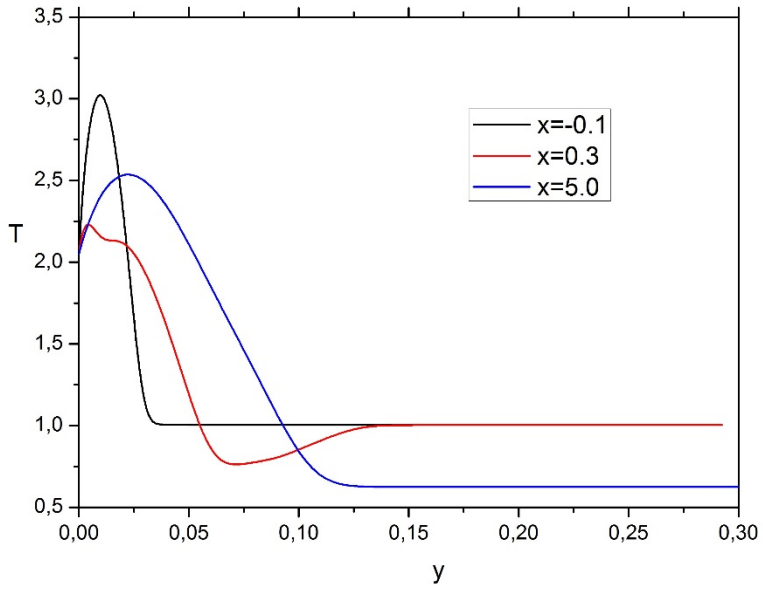

Figure 2: Boundary layer temperature profiles at various stations of *x*. Case $\theta = 10^0$.

4. e-N calculations

Stability computations were performed with the e-N method discussed above. The stability module of the HSFlow package [23] was used to calculate N-factors of disturbances as they travel over the expansion corner. The computational routine was as follows:

DOI: 10.13009/EUCASS2019-201

1) Do a global search of unstable modes: at various stations. The wide range of frequencies were considered to find unstable waves (3) with positive growth rates.
2) Calculate N-factors for disturbances according to (11) for a set of fixed frequencies. The calculations are performed from the neutral point downstream to the end of computational domain when possible. The integration of N-factors is performed along the surface of the model.

Computations performed for a flat-plate case ($\theta = 0^0$) show that the dominant waves are plain (lateral wavenumber $\beta = 0$) second mode disturbances. This is why only plain waves are considered in Section 2. Fig. 3 shows the computed N-factors. It is seen that at the point $x = 0.0$ where the expansion would occur at non-zero θ, the N-factors are relatively large ($N_{\max} \approx 6.5$). At the end of the plate, the critical value $N_{cr} \approx 10$ is reached which is a typical value for the onset of laminar-turbulent transition dominated by second-mode disturbances in low-noise environment.

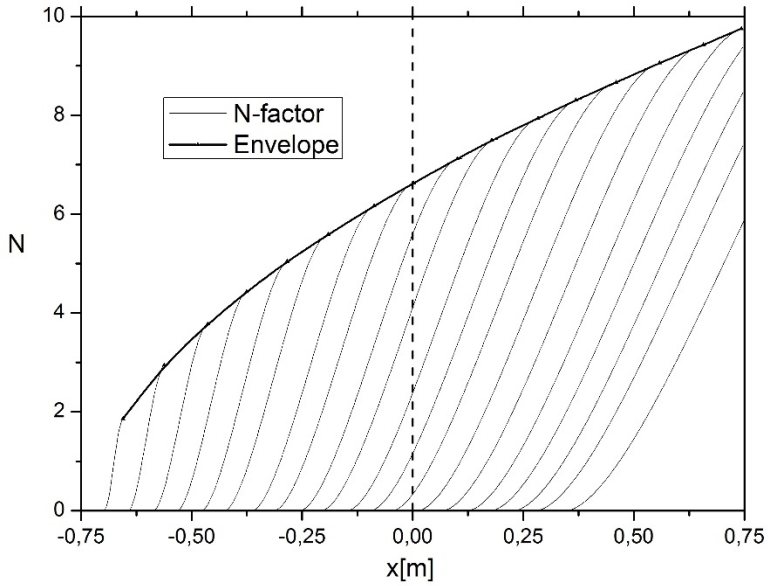

Figure 3: The N-factors for a flat plate (no expansion) case. Dashed line shows the position of the expansion corner

Computations performed for the $\theta = 5^0$ case are presented at Figure 4. It is seen that the expansion damps the high-frequency disturbances coming from a flat-plate section of the geometry (a disturbance having the highest N-factor at point $x = 0$ has the dimensional frequency $\nu^* = \omega^* / (2\pi) = 106\ kHz$). The boundary layer thickness nearly doubles after the expansion, and the set of lower frequency disturbances start to grow at the expansion part of geometry (the dimensional frequency $\nu^* = 44\,kHz$ has the highest N-factor at the end of computational domain $x = 7.5$). The damping effect of the expansion is quite strong, although it is seen that the disturbances of the second family start to grow with the increments comparable to those of disturbances at the flat plate part. It is to be noted here that the spectrum of the boundary layer becomes quite complex in the viscinity of the corner. Unstable disturbances coming from the flat-plate region synchronize with the entropy cut of the continuous spectrum. A number of new discrete modes also originate in this region. This means that in the mode branching region there different possibilities to continue the e-N calculations choosing different modes downstream of the synchronization points. This problem is discussed in Section 5.

N-factor computations performed for the case $\theta = 10^0$ are presented at Figure 6. It is seen that the further increase of the boundary layer thickness downstream of the corner point leads to the damping of the disturbances originating on the expansion part of the model. The most amplified high-frequency disturbances coming from the flat-plate part are also damped at higher rates in comparison to the case of $\theta = 5^0$. The value of N-factor for the envelope at the end of the computational domain is near 2, indicating strong damping of the linear disturbances. A similar result is observed for the case $\theta = 15^0$. Figure 7 shows the computed N-factors to the mode branching points (see Section 5).

It is important to note here that as the flow passes the corner, the spectrum of the boundary layer differs dramatically and mode branching was observed. This provides different strategies for the stability computations, as discussed below.

DOI: 10.13009/EUCASS2019-201

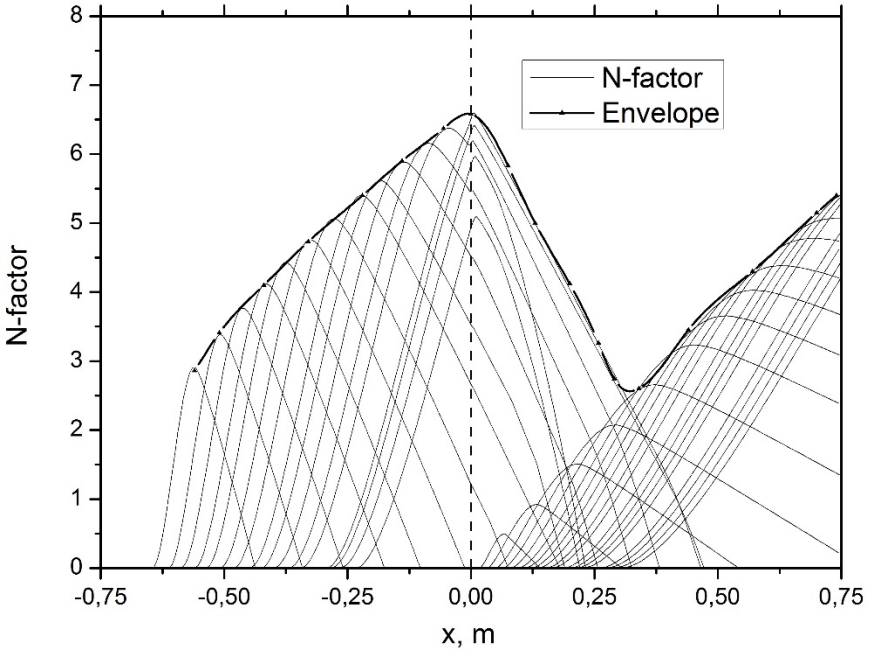

Figure 5: computed N-factors for the case $\theta = 5^0$

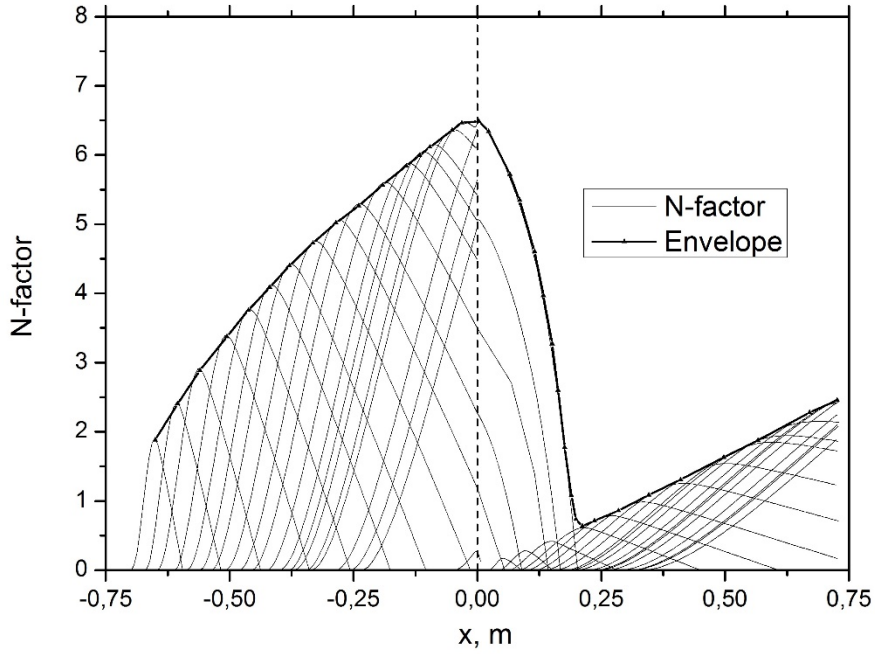

Figure 6: computed N-factors for the case $\theta = 10^0$

DOI: 10.13009/EUCASS2019-201

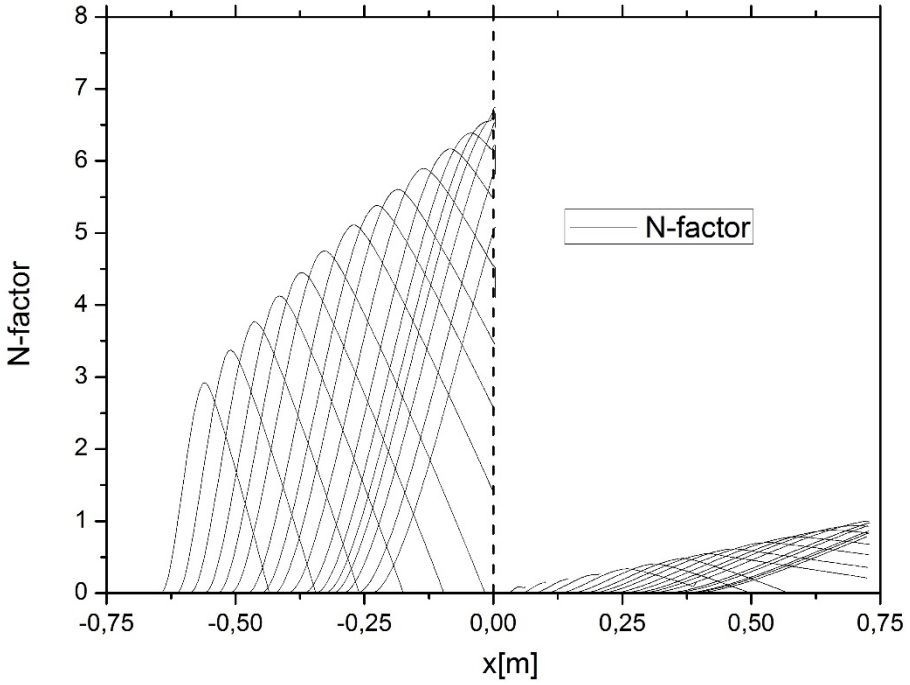

Figure 7: computed N-factors for the case $\theta = 15^0$.

5. Analysis of the boundary layer spectrum

Upstream of the expansion corner the boundary layer has the spectrum typical for cold hypersonic flat plate. Figure 8 shows the calculation of the boundary layer spectrum at the station $x = -0.01$ computed with (10).All calculations of the spectra are performed for the frequency having the largest N-factor at the point $x = 0$. The discretization has 301 points, and computational domain has approximately 5 thicknesses of the boundary layer. Nonuniform grid was used for stability computations and half of the nodes reside in the region with approximately 2 thicknesses of the boundary layer. The eigenvalues of α are made non-dimensional using the displacement thickness δ^* at the given point: $\alpha = \alpha^* \delta^*$, frequency is non-dimensionalized as follows: $\omega = \omega^* \delta^* / U_e^*$, where U_e^* is the magnitude of the velocity vector at the boundary layer edge.

Downstream the corner the spectrum changes. As one moves along the surface of the model downstream, the unstable mode moves upstream in the phase plane, and becomes stable. A set of new modes emerge on the upper phase plane, and at least one of them (the one with the smallest increment) starts to move along the slow acoustic branch. The spectrum for the section $x = 0.03$ is presented at the Figure 9

Further downstream a new discrete mode detaches from the fast acoustic branch and starts to move to the entropy/vorticity branch of the continuous spectrum. Far from the corner only one fast decaying mode is present. It is important to note here, that all the discrete modes found downstream of the corner with the frequency band coming from the flat-plate section are stable. Nevertheless, the decrements of the modes are quite different. Calculations of N-factors in this case require selection of the modes to continue computations at synchronization and/or branching points. The Figures 5-6 were obtained when calculations were performed with the most decaying discrete mode. Figure 7 was obtained when now calculations were carried out downstream of synchronization between second mode and vorticity/entropy branch of the spectrum.

DOI: 10.13009/EUCASS2019-201

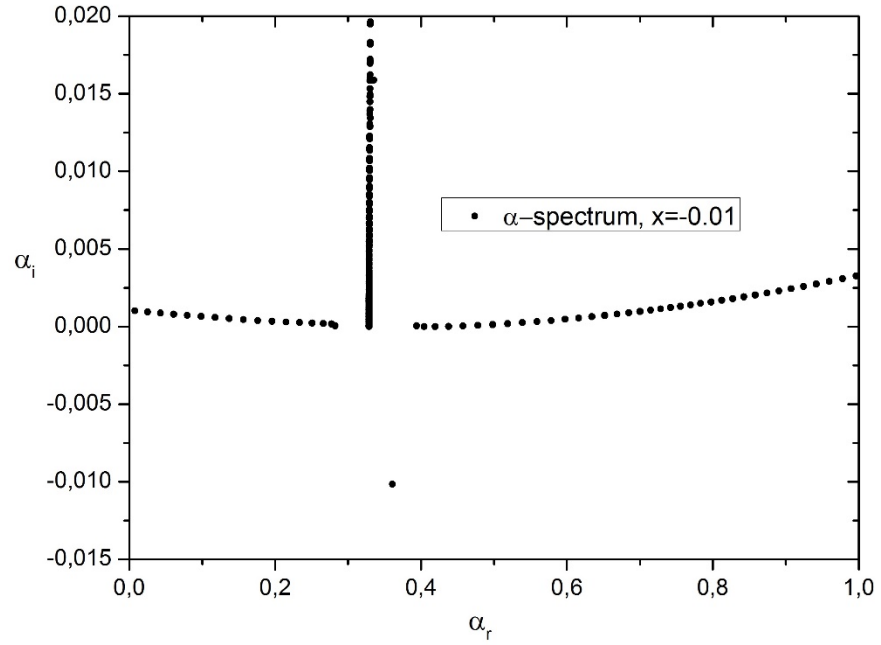

Figure 8 : Boundary layer spectrum for the station $x = -0.01$, frequency $\omega = 0.332$. Unstable discrete mode with eigen value $\alpha = 0.37 - 0.01i$ is clearly seen.

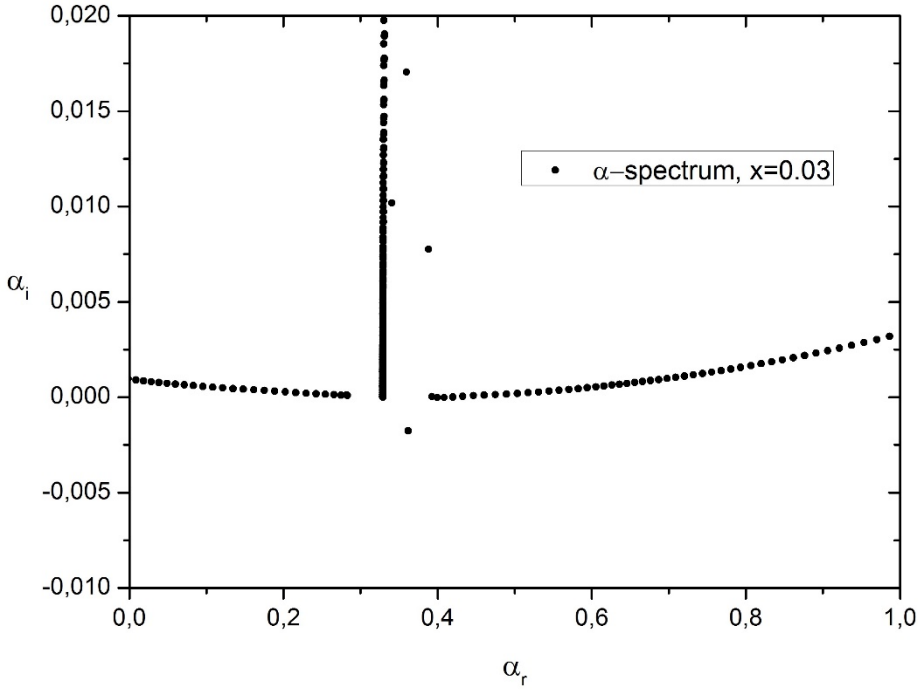

Figure 9 : Boundary layer spectrum for the station $x = -0.01$, frequency $\omega = 0.332$. Unstable discrete mode with eigen value $\alpha = 0.37 - 0.002i$ is clearly seen. Another mode with the eigen value $\alpha = 0.42 + 0.007i$ emerges.

DOI: 10.13009/EUCASS2019-201

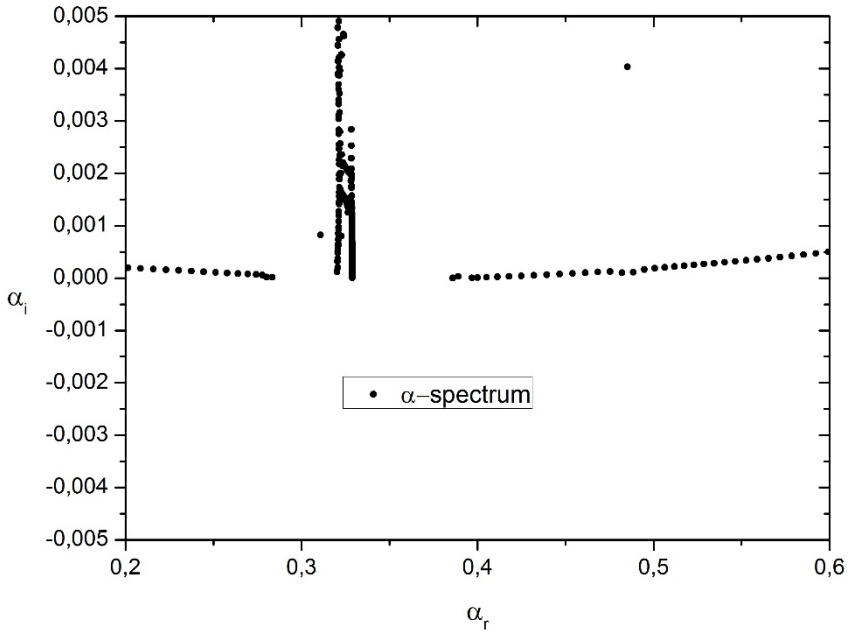

Figure 10 : Boundary layer spectrum for the station $x = 0.3$, frequency $\omega = 0.332$. The second mode enters the entropy/vorticity cut. A new mode detaches from fast acoustic branch and starts to move to the entropy/vorticity branch.

4. Conclusion

The effect of pressure gradient on the small disturbances developing in the boundary layer was considered numerically with linear stability theory. A flow past a plain expansion corner was considered. A set of expansion corners in the range 0 – 15 degrees was considered. It was shown that the expansion has the strong damping effect on the disturbances. The boundary layer spectra was analyzed in the viscinity of the expansion corner. A set of discrete modes were observed. This information will be used in the DNS computations of wave packets of disturbances passing the expansion corner.

Acknowledgments

The work has been supported by Russian foundation for basic research (project no. 18-38-20091).

References

[1] Romanenko N.P., Leontiev A.M., Solivin A.N. (1961) Investigation of drag and heat transfer for turbulent air flow in axisymmetric channels with streamwise pressure gradient // Prikladnaya Mechanika i Tekhnicheskaya Fizika, Vol. 2, no.5, pp. 16–25 (in Russian)

[2] Witte A.B., Harper E.Y. (1963) Experimental investigation of heat transfer rates in rocket thrust chambers // AIAA J., vol. 1, no. 2

[3] Deych M.E., Lazarev L.Ya. (1964) Investigation of turbulent-laminar transition of boundary layer // Ingenerno-Fizicheskiy zhurnal, vol. VII, no. 4 (in Russian)

[4] Gol'dfel'd M.A., Zinov'iev V.N., Lebiga V.A. (1987) Structure and fluctuation characteristics of a compressible turbulent boundary layer behind a fan of rarefaction waves // Fluid Dynamics, vol. 22, issue 1, pp.40–45

[5] Gillis J.C., Johnston J.P. (1983) Turbulent boundary-layer flow and structure on a convex wall and its redevelopment on a flat plate. // J. Fluid Mech., vol.135

[6] Arnette S.A., Samimy M., Elliot G.S. (1998) The effects of expansion on the turbulence structure of compressible boundary layers. // J. Fluid Mech., vol. 367

[7] Kim J., Samimy M., Lee S. (2001) Effects of compression and expansion on turbulence intensity in supersonic boundary layers. // AIAA J., vol. 39

DOI: 10.13009/EUCASS2019-201

[8] Humble R.A., Peltier S.J., Bowersox R.D.W. (2012) Visualization of the structural response of a hypersonic turbulent boundary layer to convex curvature. // Phys. Fluids, vol. 24
[9] Tichenor N.R., Humble R.A., Bowersox R.D.W. (2013) Response of a hypersonic turbulent boundary layer to favourable pressure gradients. // J. Fluid Mech., vol. 722
[10] Goldfeld M.A., Nestoulia R.V., Shiplyuk A.N. (2002) Relaminarization of turbulent boundary layer with a Mach number $M_\infty = 4$ // Journal of Applied Mechanics and Technical Physics, vol. 43, issue 1, pp. 76–82
[11] Vaganov A.V., Neyland V.Ya., Noev A.Yu., Skuratov A.S. (2015) Effect of isolated roughness on LTT in a hypersonic flow over a body of revolution with surface kinks // XI All-Russian congress on fundamental problems of theoretical and applied mechanics, Kazan, Russia
[12] Fang J., Yao Y., Zheltovodov A.A., Li Z., Lu L. (2015) Direct numerical simulation of supersonic turbulent flows around a tandem expansion-compression corner. // Phys. Fluids, vol. 27, no. 12
[13] Sun M., Hu Z., Sandham N.D. (2017) Recovery of a supersonic turbulent boundary layer after an expansion corner. // Phys. Fluids, vol. 29, no. 7
[14] Nguyen T., Behr M., Reinartz B., Hohn O., Gülhan A. (2013) Effects of sidewall compression and relaminarization in a scramjet inlet. // Journal of Propulsion and Power, vol. 29, no. 3
[15] Chuvakhov P.V., Fedorov A.V., Obraz A.O. (2018) Numerical simulation of turbulent spots generated by unstable wave packets in a hypersonic boundary layer. // Computers & Fluids, vol. 162
[16] Redford J.A., Sandham N.D., Roberts G.T. (2012) Numerical simulations of turbulent spots in supersonic boundary layers: effects of Mach number and wall temperature. // Progr Aerosp Sci, vol. 52
[17] Fedorov A., Obraz A. (2017) A hybrid LST-RANS method for modelling of laminar-turbulent transition. // 7th European Conference for Aeronautics and Space Sciences (EUCASS2017), Milan, Italy
[18] Mack L.M. (1975) A numerical method for the prediction of high-speed boundary layer tran-sition using linear theory // NASA, SP-347, p.101-123.
[19] M. R. Malik ans S.A. Orszag (1980) Efficient Computations of the Stability of 3 dimensional boundary layers// 14th Fluid Dynamics and Plasma Conference, AIAA Paper, doi 10.2514/6.1981-1277
[20] Ingen J. L. V (1956)A Suggested Semi-empirical Method for the Calculation of the Boundary Layer Region // TU Delft, VTH17
[21] Smith A. M. O. and Gamberoni N.(1956) Transition, Pressure Gradient and Stability Theory// Douglas Aircraft Company, ES 26388
[22] I. V. Egorov and A. V. Novikov (2016)Direct numerical simulation of laminar–turbulent flow over a flat plate at hypersonic flow speeds // Computational Mathematics and Mathematical Physics, vol. 56, no. 6
[23] A.O. Obraz¤ and A.V. Fedorov (2017) the hig-speed flow stability (HSFS) software package for stability analysis of compressible boundary layers // TsAGI Science Journal, vol.48, no.3